Available online at www.sciencedirect.com

SciVerse ScienceDirect

Ceramics International 39 (2013) 5785–5793

CERAMICS INTERNATIONAL

www.elsevier.com/locate/ceramint

Hydrothermal preparation, characterization and photocatalytic activity of TiO_2/Fe–TiO_2 composite catalysts

Hongxia Meng[a], Bingbing Wang[a], Song Liu[a,b,*], Rongying Jiang[a], Hong Long[c]

[a]*Department of Applied Chemistry, South China University of Technology, Guangzhou 510640, PR China*
[b]*The Key Laboratory of Fuel Cell Technology of Guangdong Province, Guangzhou 510640, PR China*
[c]*Guangdong Zhuhai Testing Institute for Quality and Metrology Supervision, Zhuhai 510900, PR China*

Received 10 November 2012; received in revised form 28 December 2012; accepted 29 December 2012
Available online 12 January 2013

Abstract

Highly active TiO_2/Fe–TiO_2 composite photocatalysts with a p–n heterojunction structure have been prepared by mixing hydrothermal-derived TiO_2 and Fe–TiO_2 nano-powders followed by grinding and drying. These photocatalysts were characterized by XPS, XRD, TEM, BET, UV–vis and Fluorescence spectroscopy, and their photocatalytic activities were evaluated by the decolorization rate of methyl orange under UV irradiation. TiO_2/Fe–TiO_2 composite photocatalysts were generally shown to have a much higher photocatalytic destruction rate than pure TiO_2, mainly due to electrostatic-field-driven electron–hole separation in TiO_2/Fe–TiO_2 composites. The best TiO_2/Fe–TiO_2 composite photocatalyst with mass ratio TiO_2:0.5 at%Fe–TiO_2 of 12:1 showed approximately 3.8 times higher photocatalytic activity than undoped TiO_2.

Keywords: B. Composites; D. Titania; Hydrothermal method; Photocatalytic properties

1. Introduction

Titanium dioxide was widely applied in pollutants processing, sensors, photovoltaics and dye-sensitized solar cells due to its nontoxicity, high stability, and photoelectric properties [1–8]. However, anatase TiO_2 with a wide band-gap of 3.2 eV and low utilization of solar energy, can be active only under UV light, which requires excitation wavelengths of $\lambda < 388$ nm. In addition, the high recombination rate of photo-generated electron–hole pairs results in poor efficiency of photocatalytic reactions. In that case, improvement of photocatalytic activity of photocatalysts and utilization of solar energy became hot subjects in recent years [9]. To enhance the photocatalytic activity, several strategies have been involved such as transition metal doping [10–15], inorganic dye-sensitizing [16,17], valuable metal deposition [18,19] and coupling titania with other semiconductors [20–34].

TiO_2 was coupled with another semiconductor to make TiO_2/semiconductor composite photocatalysts, whose photocatalytic activity was usually higher than pure TiO_2 due to the formation of heterojunction between TiO_2 with the semiconductor particles [20–34]. Many TiO_2-based composite photocatalysts have been prepared including TiO_2/Fe_3O_4 [20], TiO_2/$CuBi_2O_4$ [21], TiO_2/CdS [22,23], TiO_2/ZnO [24], TiO_2/NiO [25], TiO_2/Cu_2O [26], TiO_2/Bi_2O_3 [27], TiO_2/SnO_2 [28], TiO_2/WO_3 [29], TiO_2/$LaVO_4$ [30], TiO_2/$InVO_4$ [31], TiO_2/BDD [32,33], TiO_2/$FeTiO_3$ [34], TiO_2(B)/Fe–TiO_2 [35] and $CuInS_2$/TiO_2 [36]. These composites tend to show higher photoactivity in comparison to single-phase titania materials.

Iron was frequently employed owing to its unique half-filled electronic configuration [37], which might narrow the energy gap through formation of new impurity energy levels and effectively inhibit electron–hole recombination [38,39]. Titanium dioxide and doped titania can be prepared by several methods, such as sol–gel [40–42], co-precipitation [43] and hydrothermal [11,44,45] methods.

*Corresponding author at: Department of Applied Chemistry, South China University of Technology, Guangzhou 510640, PR China.
Tel.: +86 20 8711 4875; fax: +86 20 871 12906.
E-mail address: chsliu@scut.edu.cn (S. Liu).

0272-8842/$ - see front matter © 2013 Elsevier Ltd and Techna Group S.r.l. All rights reserved.
http://dx.doi.org/10.1016/j.ceramint.2012.12.098

In previous paper [46,47], we have prepared TiO_2 and doped TiO_2 powders by sol–gel method. In the present paper we prepared TiO_2 and Fe-doped TiO_2 nano-powders with hydrothermal method, a low-power method without high-temperature calcination. TiO_2/Fe–TiO_2 composite photocatalysts were synthesized by coupling hydrothermal-derived Fe–TiO_2 with TiO_2 in order to promote the formation of p–n heterojunction to enhance the photocatalytic activity. The as-prepared photocatalysts were characterized and investigated by photocatalytic decolorization of methyl orange under UV irradiation.

2. Experimental

2.1. Preparation

Pure titania catalyst was synthesized by hydrothermal method using tetrabutyl titanate as a titanium precursor. 8.5 mL tetrabutyl titanate (CP, Shanghai Chemical Reagent Co.) was added drop-wise into 45 mL deionized water under vigorous stirring. The resulting suspension was still stirred for 12 h, then moved to a teflon vessel and put in a stainless steel autoclave to carry out hydrothermal treatment at 200 °C for 24 h. The stainless steel autoclave was then opened at room temperature and the precipitates were separated and washed with deionized water for three times. The as prepared precipitates were dried at 80 °C and then grounded to obtain fine titania powders finally.

Several Fe-doped TiO_2 powders were generated by hydrothermal method. 8.5 ml tetrabutyl titanate (CP, Shanghai Chemical Reagent Co.) was added drop-wise into 45 mL $Fe(NO_3)_3$ solution under vigorous stirring. The following procedures were carried according to the pure titania. The Fe^{3+}–TiO_2 catalysts had a nominal atomic ratio (Fe/Ti) of x%, so they are named as x%Fe–TiO_2 in this study.

Composite photocatalysts were prepared by coupling undoped TiO_2 with Fe-doped TiO_2 nano-powder. Pure TiO_2 and x%Fe–TiO_2 nano-powder were mixed at a mass ratio of 12:1, and then grounded with 5 ml deionized water in mortar for 2 h. Finally the mixture was dried at 200 °C, and grounded to obtain a series of composite photocatalysts named as TiO_2/x%Fe–TiO_2.

2.2. Characterization

Chemical compositions of composites were analyzed through X-ray photoelectron spectroscopy (VG Scientific, Kratos Axis Ultra, power 300-W, monochromatic Al Kα X-ray source). All binding energies were referenced to the C1s peak (284.6 eV) arising from adventitious carbon. X-ray diffraction (XRD) patterns were collected from 10° to 80° in 2θ with a scan rate of 0.02° steps/s using a Bruker D8 Advance diffractometer with Ni-filtered Cu Kα as radiation source ($\lambda = 0.15418$ nm) at 40 kV and 36 mA. The average crystal sizes were calculated from the X-ray diffractograms by the Scherrer formula. A transmission electron microscope (TEM), JEM-2010, was applied to observe the morphology of catalysts and estimate the particle size. The surface area of catalysts was determined using a standard Brunauer–Emmett–Teller (BET) apparatus (Micromeritics TristarII3020). The pore size distribution of the catalysts was determined by the Barrett–Joyner–Halenda (BJH) method. The UV–visible diffuse reflectance spectra were recorded on a Hitachi UV-3010 spectrometer equipped with an integrating sphere, while $BaSO_4$ was used as the reference material. Photoluminescence spectra were collected on a Hitachi F-4500 Fluorescence spectrometer with a powder holder accessory under room temperature, and the emission spectra were collected between 350 nm and 600 nm.

2.3. Photocatalytic activity measurements

Photocatalytic decolorization of methyl orange in an aqueous medium was used as a probe reaction to access the photocatalytic activity of all powders. A Pyrex cylindrical photoreactor with an effective volume of 250 mL was used to conduct photocatalytic degradation experiments, which was surrounded by a Pyrex circulating water jacket. An 8-W UV lamp (Toshiba, Inc.) with a main emission at 365 nm was positioned at the center of the cylindrical vessel and used for photoreaction. For each experiment, 0.2 g of photocatalyst was added to 250 mL of 5 mg/L methyl orange solution stirred with a magnetic stirrer. The aerated suspension was first stirred for 30 min to reach adsorption equilibrium of methyl orange without UV-light exposure. Following this, the photocatalytic reaction was started by the exposure of UV-light. After a setup exposure time, 10 mL suspension was sampled, centrifuged, and measured the absorbance at 464 nm with a Hitachi UV-3010 spectrometer. The blank test was also carried out by irradiating methyl orange solution without photocatalyst.

3. Results

3.1. Characterization of photocatalysts

Fig. 1 shows XPS spectra of Ti 2p and O 1s of photocatalysts. There are slight differences in the locations of binding energy of Ti $2p_{3/2}$ among different samples. The Ti $2p_{3/2}$ line is found at an electron binding energy (BE) of 458.4 eV on the undoped TiO_2, and it shifts slightly 0.2 eV to higher electron binding energy upon iron doping (2% Fe–TiO_2). The O 1s peak at 529.7 eV on the undoped TiO_2 is corresponding to bulk oxide (O^{2-}) in TiO_2 lattice [48], which shifts slightly to higher electron binding energy upon iron doping. This phenomenon may be attributed to the formation of Ti–O–Fe bonds in the crystal lattice [1,49]. The shift of O 1s and Ti $2p_{3/2}$ XPS lines of TiO_2/0.5% Fe–TiO_2 by an amount of 0.3 eV to lower BE is induced by a simple shift of the Fermi level into TiO_2 band gap [50]. In addition, there is no signal of iron for iron containing TiO_2, due to the low iron content.

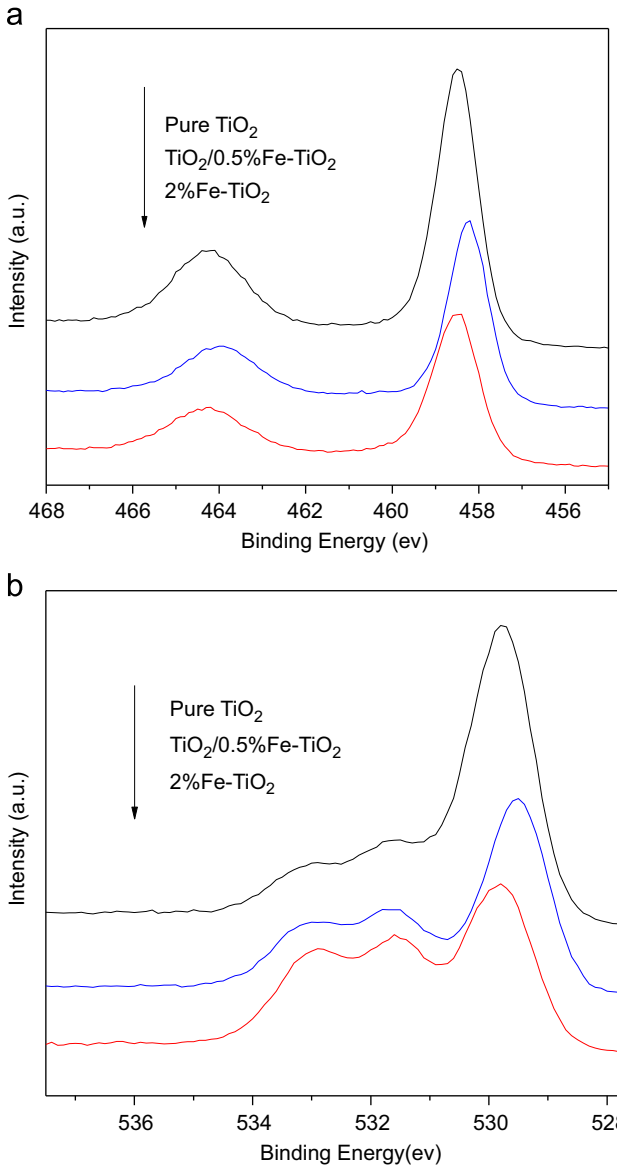

Fig. 1. XPS spectra of Ti 2p (a) and O 1s (b) of TiO_2, 2% Fe–TiO_2 and TiO_2/0.5% Fe–TiO_2.

XRD patterns of TiO_2-based nanoparticles are shown in Fig. 2. The characteristic peaks of all samples positioned at $2\theta = 25.3^\circ$, 37.7° and 48.0° are assigned to (101), (004) and (200) planes of anatase-TiO_2, respectively. No significant characteristic peaks of iron oxide were detected, indicating the formation of no single iron oxide phase. This may be ascribed to the low Fe content that was beyond detection by XRD or the entrance of Fe^{3+} (64 pm) into TiO_2 crystal lattice to substitute Ti^{4+} (68 pm) due to their very close radius [42,49]. Such a substitution restrains the growth of TiO_2 crystallite [46,51]. Based on the Debye–Sherrer equation, the average crystallite sizes of all samples are listed in Table 1. It is noted that the average crystallite sizes of Fe-doped TiO_2 and TiO_2/Fe–TiO_2 composites decreased with the increase of Fe dopant concentration. This can be due to the possible formation of Fe–O–Ti bonds which inhibits the growth of crystal grains [52].

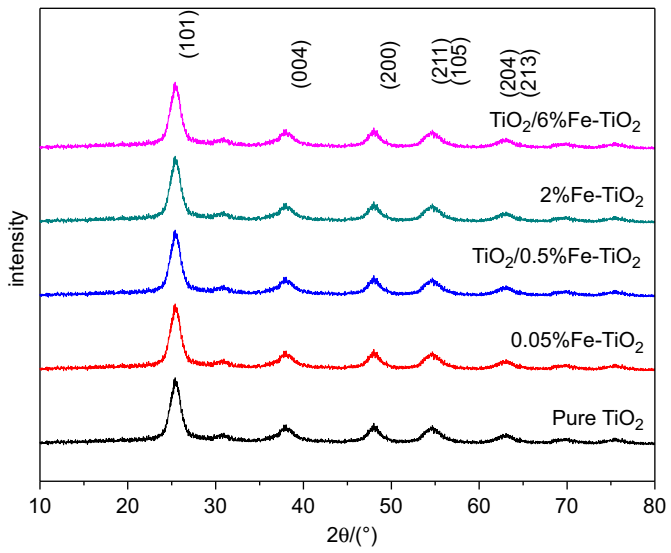

Fig. 2. XRD patterns of catalysts.

TEM images in Fig. 3 reveal that the prepared samples consisted of aggregates of primary particles of 5–10 nm in diameter, which is in general agreement with the XRD determination.

The N_2 adsorption–desorption isotherms of catalysts in Fig. 4a are characteristic type-IV curves according to BDDT classification with hysteresis loops [53], indicating the existence of mesoporous structure in catalysts. The BET surface areas of TiO_2-based samples are summarized in Table 1. Compared to pure TiO_2, there are not significant changes of surface area for Fe–TiO_2, while TiO_2/Fe–TiO_2 composites exhibited lower surface area than pure TiO_2 due to the coupling or drying. The BJH pore size distributions (Fig. 4b) calculated on the basis of desorption branches of isotherms show that the average pore diameter was 4.5–5.5 nm. The formation of mesoporous structure in samples is attributed to the aggregation of TiO_2 crystallites [54].

Fig. 5 displays UV–vis DRS of TiO_2-based photocatalysts with inset showing plot of $(\alpha h\nu)^{1/2}$ versus energy ($h\nu$). As observed in Fig. 5, the absorption edge of undoped TiO_2, appeared at about 400 nm, corresponding to the band gap energy of about 3.1 eV. This value was close to the reported value of anatase (3.2 eV) [55]. Compared with undoped TiO_2, iron (III)-doping titania and TiO_2/Fe–TiO_2 composite catalysts show enhanced absorptions in the range from 400 to 600 nm with increasing Fe content, accompanied with the changes on color from white to reddish yellow. The absorption edge of 2% Fe–TiO_2 and 4% Fe–TiO_2 appeared at about 440 nm and 520 nm, corresponding to the band gap energy of about 2.8 eV and 2.4 eV respectively. The red shift of the spectra can be ascribed to the formation of a dopant energy level [20,49] within TiO_2 band gap after Fe-doping. Fe^{3+} impurity energy level is close to the valance band of TiO_2, so the electron would rather transfer from the Fe^{3+} impurity level than from the valance band to conduction band due

Table 1
Physicochemical properties and photocatalytic activities of the catalysts.

Sample	Specific surface area (m^2/g)	Apparent rate constant K(min^{-1})	Crystal size (nm)
Pure TiO_2	203.5	0.0467	7.1
0.01% Fe–TiO_2	205.6	0.0525	
0.05% Fe–TiO_2	200.7	0.0482	6.3
0.1% Fe–TiO_2	196.5	0.0377	
0.5% Fe–TiO_2	208.9	0.0150	
1% Fe–TiO_2	208.9	0.0101	
2% Fe–TiO_2	219.1	0.0081	5.3
4% Fe–TiO_2	236.6	0.0074	
6% Fe–TiO_2	211.3	0.0050	
8% Fe–TiO_2	211.0	0.0037	
TiO_2/0.01% Fe–TiO_2	176.2	0.0520	
TiO_2/0.05% Fe–TiO_2	153.6	0.0581	
TiO_2/0.1% Fe–TiO_2	163.5	0.0716	
TiO_2/0.5% Fe–TiO_2	165.9	0.1771	6.1
TiO_2/1% Fe–TiO_2	166.4	0.0896	
TiO_2/2% Fe–TiO_2	166.1	0.0739	
TiO_2/4% Fe–TiO_2	159.4	0.0660	
TiO_2/6% Fe–TiO_2	158.2	0.0497	5.5
Mechanical mixture[a]		0.0467	

[a]The molar ratio of undoped TiO_2 to 0.5% Fe–TiO_2 is 12.

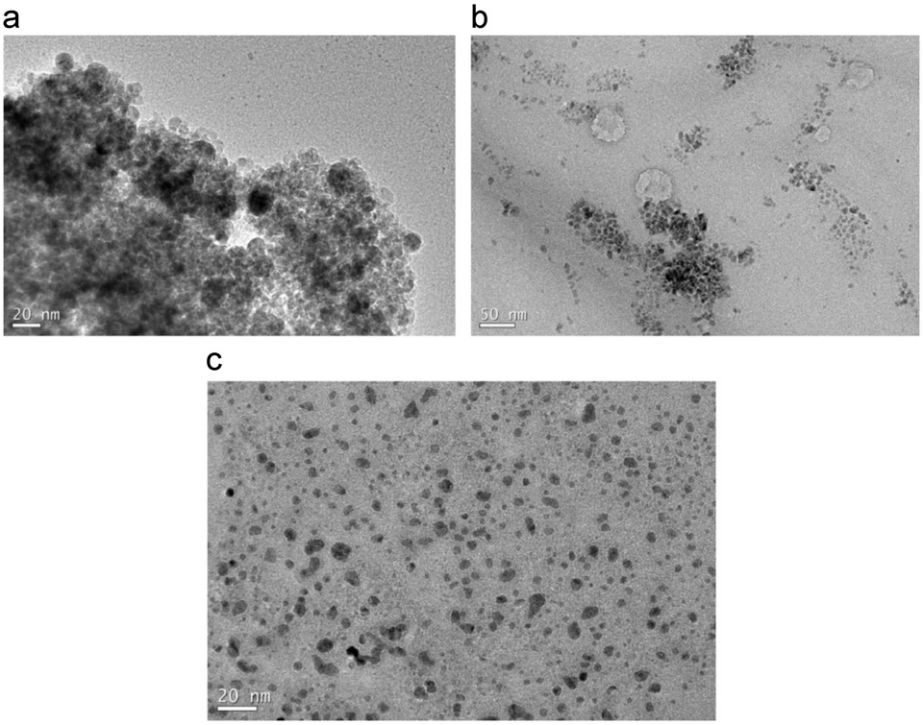

Fig. 3. TEM images of: (a) TiO_2, (b) 2% Fe–TiO_2 and (c) TiO_2/0.5% Fe–TiO_2.

to the lower excitation energy, which effectively red shift the band edge absorption [12]. In addition, the d–d transition $^2T_{2g} \rightarrow {}^2A_{2g}$, $^2T_{1g}$ of Fe^{3+} or the charge transfer transition between iron ions ($Fe^{3+} + Fe^{3+} \rightarrow Fe^{2+} + Fe^{4+}$) contribute to the enhanced absorption in visible region [44]. Thus, optical absorption of iron doped systems depends on Fe energy levels within TiO_2 lattice, d electronic configuration and the distribution of dopants iron ions.

Photoluminescence spectra (PL) of catalysts in Fig. 6 exhibits six main emission peaks at about 399, 422, 452, 469, 483 and 493 nm with excitation at 320 nm. The peak positions of iron doped catalysts are in agreement with pure TiO_2, indicating no other new luminescence is induced

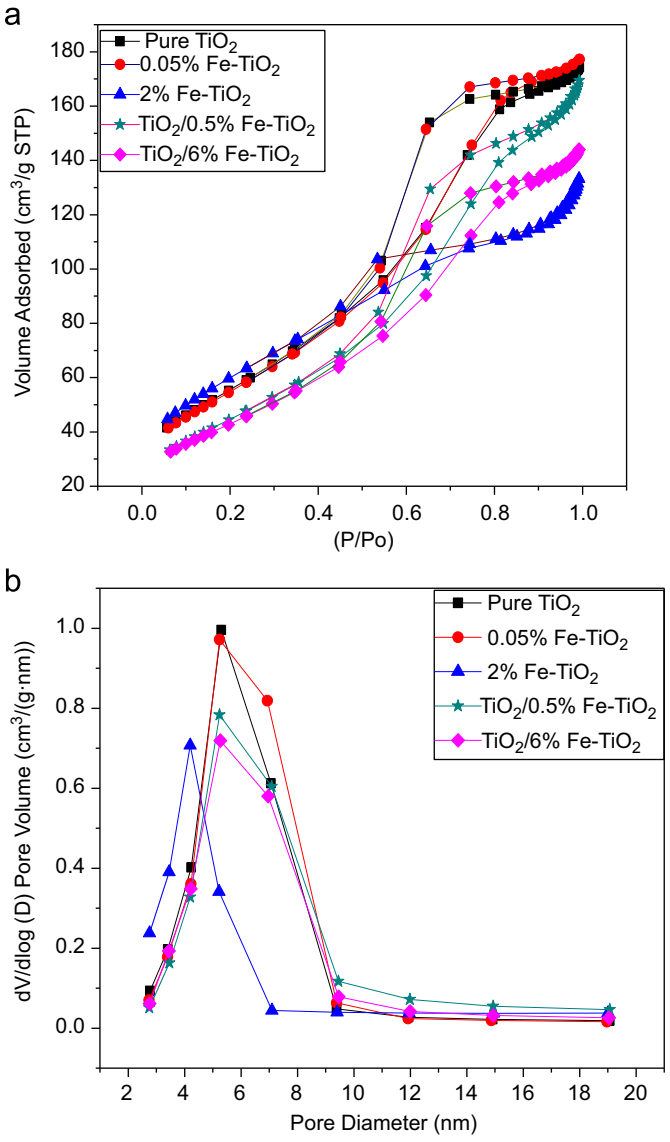

Fig. 4. Nitrogen adsorption–desorption isotherms (a) and pore size distribution curve of the catalysts (b).

by iron-doping. High-energy peaks can be assigned to band edge luminescence of TiO_2 particles, while lower energy peaks are introduced by the presence of oxygen vacancies [56,57]. The PL intensities of TiO_2-based catalysts are quite sensitive to iron doping and decrease with increasing Fe content. The great decrease in emission intensity of 2% Fe–TiO_2 compared with undoped TiO_2 may be due to the impurity levels introduced by dopant that enhanced non-radiative recombination of the excited electrons [12,58]. Similar quenching in the luminescence intensity has also been observed for V-, Fe-, W-, Zr-, Cu-, Ni-, Ga-, Cd-, Ag-, Al- and Pb-doped TiO_2 by Nagaveni et al. [12], Zhou et al. [59], and Rahman et al. [58].

3.2. Photocatalytic activity

Fig. 7a and b displays the decrease of methyl orange concentration as a function of UV light irradiation time over TiO_2-based photocatalysts. The blank test shows that photo-induced self-sensitized photo decolorization has little influence on the results of experiment. The photocatalytic decolorization of methyl orange is an apparent first-order reaction verified by the linear transforms $\ln c_0/c = Kt$ illustrated in the insert in Fig. 7c and d. To enable quantitative comparison, the apparent rate constants (displayed in Table 1 and Fig. 7) were calculated to represent the photoactivities. TiO_2/0.5% Fe–TiO_2 had the best photocatalytic activity whose apparent rate constant was about 3.8 times as large as that of undoped TiO_2.

4. Discussion

Iron ions can introduce energy levels into the band-gap, which are responsible for the red shift of intrinsic absorption edge of TiO_2 and the enhancement of visible light adsorption. However, there is no direct correlation between the light absorption ability and photocatalytic rate, electronic structure seems more important to the photocatalytic activity of TiO_2 samples [60]. Dopant iron ion, acting as mediators, affects the process of charge separation, charge-carrier recombination and interfacial charge transfer of TiO_2-based catalysts [60]. As presented in Table 1, Fig. 7a and Fig. 7c, the photocatalytic activity of x% Fe–TiO_2 with lower dopant level (not more than 0.05%) is better than undoped TiO_2, while with higher dopant level the activity is worse. In iron-doped titania, Fe^{3+} may act as photogenerated electron trappers because relatively unstable Fe^{2+} (d^6) tend to be oxidized to half-filled high spin of Fe^{3+} (d^5) by transferring electrons to adsorbed O_2 on the surface of TiO_2 or to a neighboring Ti^{4+}surface, which then lead to interfacial electron transfer [60,61]. Therefore, rapid transport of photogenerated carriers could be achieved, and an effective charge separation was subsequently accomplished. These superior properties contributed to the enhancement of photocatalytic activity [62]. Unfortunately, Fe^{3+} can also act as the recombination center for the photogenerated electrons and holes. When the doping concentration was too high, the recombination increased and competed with the redox processes due to the decreasing distance between trapping sites [1,61], which was detrimental to the photocatalytic activity, though heavy doped samples could absorb more photons.

As presented in Table 1, Fig. 7b and d, all TiO_2/Fe–TiO_2 photocatalysts had higher photocatalytic activity than undoped TiO_2. Liau et al. [63] have prepared nano-TiO_2 electrode by coating Fe-doped TiO_2 film on top of undoped TiO_2 film. The electrode give a strong rectifying action, which is the characteristic of a p–n junction, i.e. a p–n junction can be formed at the interfaces between TiO_2 with Fe–TiO_2 particles. Anatase TiO_2 is an n-type semiconductor [63–65]; whereas, iron ion doped titanium dioxide is taken as a p-type semiconductor [66]. Electrical and thermoelectric power measurements showed that the electrical conduction changed from n-type conduction for

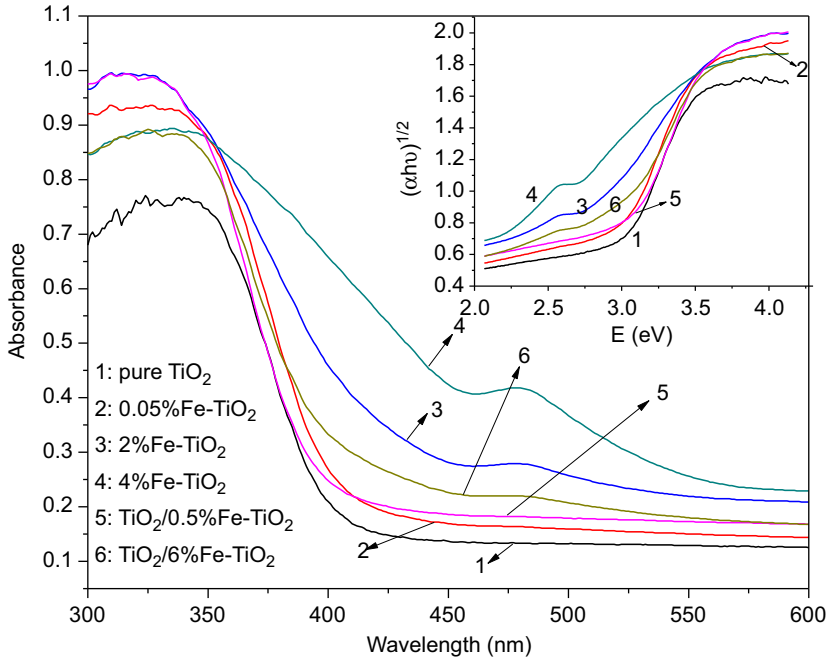

Fig. 5. UV–vis DRS spectra of catalysts.

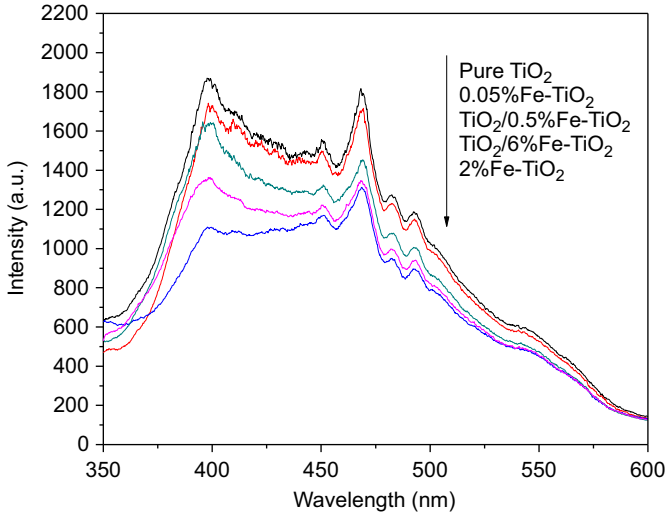

Fig. 6. FS spectra of catalysts.

undoped TiO_2 to p-type conduction for doped TiO_2 [66]. In Fe–TiO_2, iron ions act as acceptor impurities [66–68], and electrons given up by oxygen vacancies (donor) are compensated by iron ions (acceptor). In this study, TiO_2/Fe–TiO_2 photocatalysts are the composite containing Fe–TiO_2 and undoped titania (anatase) nanoparticles. At the interface between Fe–TiO_2 and undoped titania particles, a p–n heterojunction has been formed. At a p–n heterojunction located at the juncture between Fe–TiO_2 and anatase, electrons diffuse from anatase into Fe–TiO_2 region, creating an accumulation of negative charges in Fe–TiO_2 region and a positive section in anatase region in the vicinity of the junction. This sets up an internal electrostatic field directed from anatase to Fe–TiO_2 region, creating an energy barrier for the electron transfer from anatase to Fe–TiO_2 [69]. Under irradiation, both Fe–TiO_2 and undoped anatase titania nanoparticles absorb the band-gap photos and then the electron–hole pairs are generated. Photogenerated holes and electrons separate under the influence of internal electrostatic field in the p–n heterojunction region. Holes move to Fe–TiO_2 side, and electrons to pure TiO_2 side. Thereby, the chance of electron–hole recombination is reduced. This leads to high photocatalytic activity of photocatalytic decolorization of methyl orange [65,47]. The p–n heterojunction formation model and schematic diagram of built-in electric field are illustrated in Fig. 8.

The built-in electric field strength of space-charge region in p–n heterojunction increases with the increase of absolute value of difference of Fermi energy between the materials on the two sides. The Fermi energy of Fe-doped titania decreases with the increase of iron dopant concentration. So, with increasing iron dopant concentration, the built-in electric field strength increases and therefore the photo-generated electron–hole pairs separate more quickly under illumination. On the other hand, the spike formed in the conduction band at the interface may prevent flow of photo-generated electrons [69,70]. The higher the iron dopant concentration is, the larger the conduction band edge discontinuity is. Therefore, for composite photocatalysts with higher iron dopant concentration, the conduction-band spike barrier is relatively larger, which is detrimental to the photocatalytic activity. In additional, for samples with higher iron dopant concentration, dopants act more as recombination centers than as trap sites for charge transfer, which leads to the reduced activity

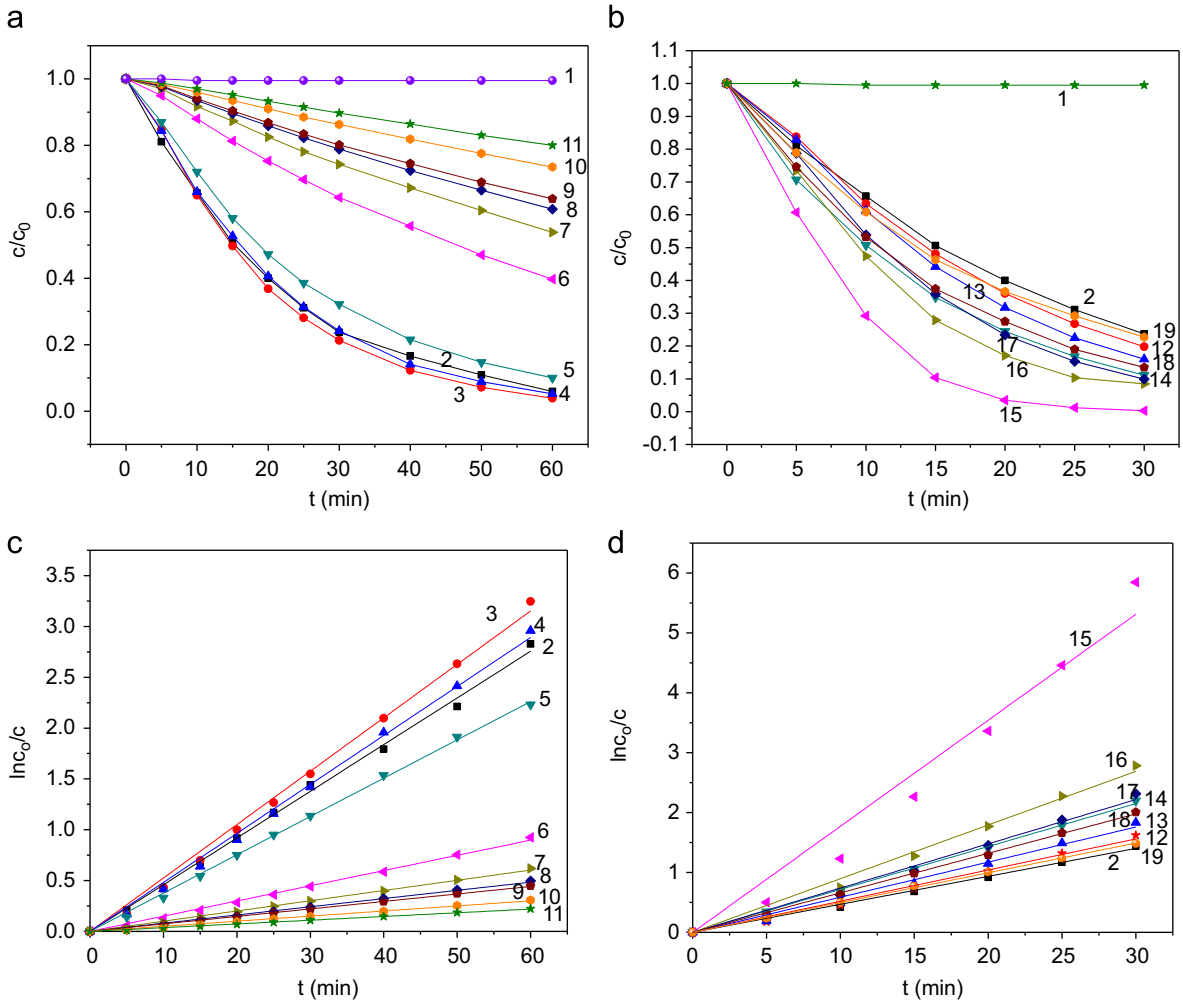

Fig. 7. Decrease of methyl orange concentration as a function of UV irradiation time over the different catalysts: (1) No catalysts, (2) Pure TiO_2, (3) 0.01% Fe–TiO_2, (4) 0.05 Fe–TiO_2, (5) 0.1% Fe–TiO_2, (6) 0.5% Fe–TiO_2, (7) 1% Fe–TiO_2, (8) 2% Fe–TiO_2, (9) 4% Fe–TiO_2, (10) 6% Fe–TiO_2, (11) 8% Fe–TiO_2, (12) TiO_2/0.01% Fe–TiO_2, (13) TiO_2/0.05% Fe–TiO_2, (14) TiO_2/0.1% Fe–TiO_2, (15) TiO_2/0.5% Fe–TiO_2, (16) TiO_2/1% Fe–TiO_2, (17) TiO_2/2% Fe–TiO_2, (18) TiO_2/4% Fe–TiO_2, (19) TiO_2/6% Fe–TiO_2.

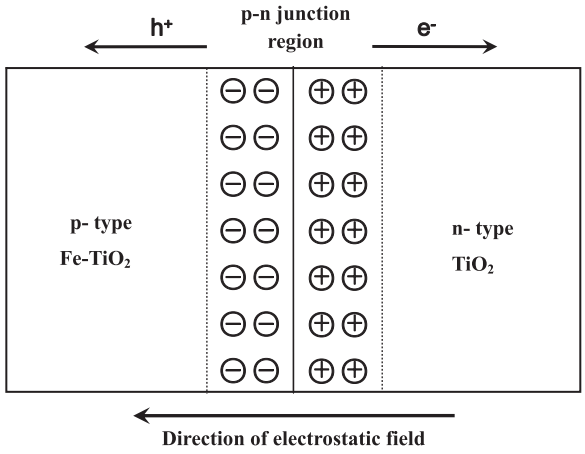

Fig. 8. p-n junction formation model and the schematic diagram of build-in electric field.

in spite of they can absorb more of the photons, which is beneficial to the photoactivity [60]. So an optimal iron dopant concentration (0.5% in this study) in TiO_2/Fe–TiO_2 composite photocatalysts exists for maximum photocatalytic efficiency.

A mechanical mixture of undoped TiO_2 and 0.5% Fe–TiO_2 was also tested for photocatalytic decolorization (the molar ratio of undoped TiO_2 to 0.5% Fe–TiO_2 is 12). The photocatalytic activity of the mechanical mixture as listed in Table 1 was the same as that of the pure TiO_2, indicating that the intimate contact between undoped TiO_2 with 0.5% Fe–TiO_2 was crucial for the formation of p–n heterojunction.

5. Conclusion

Highly active TiO_2/Fe–TiO_2 composite photocatalysts with a p–n heterojunction structure have been prepared by mixing hydrothermal-derived TiO_2 and Fe–TiO_2 nano-powders followed by grinding and drying. TiO_2/Fe–TiO_2 composite catalysts were generally shown to have a higher photocatalytic destruction rate than pure TiO_2 mainly due to electrostatic-field-driven electron–hole separation in

TiO_2/Fe–TiO_2 composite photocatalysts. An optimal iron dopant concentration (0.5% in this study) in TiO_2/Fe–TiO_2 composite photocatalysts exists for maximum photocatalytic efficiency.

Acknowledgment

This work was supported under open fund awarded by the Key Laboratory of Fuel Cell Technology of Guangdong Province.

References

[1] N.R. Khalid, Z.L. Hong, E. Ahmed, Synergistic effects of Fe and graphene on photocatalytic activity enhancement of TiO_2 under visible light, Applied Surface Science 258 (2012) 5827–5834.
[2] L. Gu, Z.X. Chen, C. Sun, B. Wei, X. Yu, Photocatalytic degradation of 2,4-dichlorophenol using granular activated carbon supported TiO_2, Desalination 263 (2010) 107–112.
[3] A.C. Rodrigues, M. Boroski, N.S. Shimada, J.C. Garcia, J. Nozaki, N. Hioka, Treatment of paper pulp and paper mill wastewater by coagulation–flocculation followed by heterogeneous photocatalysis, Journal of Photochemistry and Photobiology, A 194 (2008) 1–10.
[4] M.R. Hoffmann, S.T. Martin, W. Choi, D.W. Bahnemann, Environmental applications of semiconductor photocatalysis, Chemical Reviews 95 (1995) 69–96.
[5] M. Grätzel, Conversion of sunlight to electric power by nanocrystalline dye-sensitized solar cells, Journal of Photochemistry and Photobiology A 164 (2004) 3–14.
[6] G.H. Liu, K.Y. Wang, N. Hoivik, H. Jakobsen, Progress on free-standing and flow-through TiO_2 nanotube membranes, Solar Energy Materials and Solar Cells 98 (2012) 24–38.
[7] S.G. Pawar, M.A. Chougule, V.B. Patil, Development of nanostructured polyaniline–titanium dioxide gas sensors for ammonia recognition, Journal of Applied Polymer Science 125 (2012) 1418–1424.
[8] C.J. Barbe, F. Arendse, P. Comte, M. Jirousek, F. Lenzmann, V. Shklover, M. Grätzel, Nanocrystalline titanium oxide electrodes for photovoltaic applications, Journal of the American Ceramic Society 80 (1997) 3157–3171.
[9] S.F. Chen, L. Chen, S. Gao, G.Y. Cao, The preparation of nitrogen-doped photocatalyst $TiO_{2-x}N_x$ by ball milling, Chemical Physics Letters 413 (2005) 404–409.
[10] C.F. Wu, W.P. Qin, G.H. Qin, S.H. Huang, J.S. Zhang, D. Zhao, Near-infrared-to-visible photon upconversion in Mo-doped rutile titania, Chemical Physics Letters 366 (2002) 205–210.
[11] V.N. Nguyen, N.K.T. Nguyen, P.H. Nguyen, Hydrothermal synthesis of Fe-doped TiO_2 nanostructure photocatalyst, Advances in Natural Sciences: Nanoscience and Nanotechnology 2 (2011) 1–4.
[12] K. Nagaveni, M.S. Hegde, Giridhar Madras, Structure and photocatalytic activity of $Ti_{1-x}M_xO_{2\pm\delta}$ (M=W, V, Ce, Zr, Fe, and Cu) synthesized by combustion method, Journal of Physical Chemistry B 108 (2004) 20204–20212.
[13] S. George, S. Pokhrel, Z.X. Ji, B.L. Henderson, T. Xia, L.J. Li, J.I. Zink, L. Madler, Role of Fe doping in tuning the band gap of TiO_2 for the photo-oxidation-induced cytotoxicity paradigm, Journal of the American Chemical Society 133 (2011) 11270–11278.
[14] S. Liu, J.T. Wu, X.P. Liu, R.Y. Jiang, TiO_2/V–TiO_2 composite photocatalysts with an n–n heterojunction semiconductor structure, Journal of Molecular Catalysis A: Chemical 332 (2010) 84–92.
[15] S.M. Karvinen, The effects of trace element doping on the optical properties and photocatalytic activity of nanostructured titanium dioxide, Industrial and Engineering Chemistry Research 42 (2003) 1035–1043.
[16] C.Y. Wang, J. Li, S.Y. Cai, Performance improvement of dye-sensitizing solar cell by semi-rigid triarylamine-based donors, Dyes and Pigments 94 (2012) 40–48.
[17] F. Wang, S.X. Min, Y.Q. Han, L. Feng, Visible-light-induced photocatalytic degradation of methylene blue with polyaniline-sensitized composite photocatalysts, Superlattices and Microstructures 48 (2010) 170–180.
[18] S. Obregón Alfaro, V. Rodríguez-Gonzálezb, A.A. Zaldívar-Cadena, S.W. Lee, Sonochemical deposition of silver–TiO_2 nanocomposites onto foamed waste-glass: evaluation of Eosin Y decomposition under sunlight irradiation, Catalysis Today 166 (2011) 166–171.
[19] Y.F. Yang, P. Sangeetha, Y.W. Chen, Au/TiO_2 catalysts prepared by photo-deposition method for selective CO oxidation in H_2 stream, International Journal of Hydrogen Energy 34 (2009) 8912–8920.
[20] Z.L. Shi, C. Du, S.H. Yao, Preparation and photocatalytic activity of cerium doped anatase titanium dioxide coated magnetite composite, Journal of the Taiwan Institute of Chemical Engineers 42 (2011) 652–657.
[21] W. Liu, S. Chen, S. Zhang, W. Zhao, H. Zhang, X. Yu, Preparation and characterization of p–n heterojunction photocatalyst p-$CuBi_2O_4$/n-TiO_2 with high photocatalytic activity under visible and UV light irradiation, Journal of Nanoparticle Research 12 (2010) 1355–1359.
[22] N. Serpone, P. Maruthamuthu, P. Pichat, et al., Exploiting the interparticle electron transfer process in the photocatalysed oxidation of phenol, 2-chlorophenol and pentachlorophenol:chemical evidence for electron and hole transfer between coupled semiconductors, Journal of Photochemistry and Photobiology A 85 (1995) 247–255.
[23] A.H. Zyoud, N. Zaatar, I. Saadeddin, C. Ali, D. Park, G. Campet, H.S. Hilal, CdS-sensitized TiO_2 in phenazopyridine photo-degradation: catalyst efficiency, stability and feasibility assessment, Journal of Hazardous Materials 173 (2010) 318–325.
[24] S.F. Chen, W. Zhao, W. Liu, Preparation characterization and activity evaluation of p–n junction photocatalyst p-ZnO/n-TiO_2, Applied Surface Science 255 (2008) 2478–2484.
[25] S. Chen, S. Zhang, W. Liu, W. Zhao, Preparation and activity evaluation of p–n junction photocatalyst NiO/TiO_2, Journal of Hazardous Materials 155 (2008) 320–326.
[26] F.R. Xiu, F.S. Zhang, Preparation of nano-Cu_2O/TiO_2 photocatalyst from waste printed circuit boards by electrokinetic process, Journal of Hazardous Materials 172 (2009) 1458–1463.
[27] Y. Bessekhouad, D. Robert, J.V. Weber, Photocatalytic activity of Cu_2O/TiO_2, Bi_2O_3/TiO_2 and $ZnMn_2O_4$/TiO_2 heterojunctions, Catalysis Today 101 (2005) 315–321.
[28] J. Shang, W.Q. Yao, Y.F. Zhu, N.Z. Wu, Structure and photocatalytic performances of glass/SnO_2/TiO_2 interface composite film, Applied Catalysis, A 257 (2004) 25–32.
[29] T. Ohno, F. Tanigawa, K. Fujihara, S. Izumi, M. Matsumura, Photocatalytic oxidation of water on TiO_2-coated WO_3 particles by visible light using Iron(III) ions as electron acceptor, Journal of Photochemistry and Photobiology A 118 (1998) 41–44.
[30] H.J. Huang, D.Z. Li, Q. Lin, W.J. Zhang, Y. Shao, Y.B. Chen, M. Sun, Efficient degradation of benzene over $LaVO_4$/TiO_2 nanocrystalline heterojunction photocatalyst under visible light irradiation, Environmental Science and Technology 43 (2009) 4164–4168.
[31] G.C. Xiao, X.C. Wang, D.Z. Li, X.Z. Fu, $InVO_4$-sensitized TiO_2 photocatalysts for efficient air purification with visible light, Journal of Photochemistry and Photobiology A 193 (2008) 213–221.
[32] H.B. Yu, S. Chen, X. Quan, H.M. Zhao, Y.B. Zhang, Fabrication of a TiO_2-BDD heterojunction and its application as a photocatalyst for the simultaneous oxidation of an azo dye and reduction of Cr(VI), Environmental Science and Technology 42 (2008) 3791–3796.
[33] S. Chai, G. Zhao, Y. Zhang, Y.J. Wang, F.Q. Nong, M.F. Li, D.M. Li, Selective photoelectrocatalytic degradation of decalcitrant contaminant driven by an n–P heterojunction nanoelectrode with molecular recognition ability, Environmental Science and Technology 46 (2012) 10182–10190.
[34] F. Ye, A. Ohmori, C. Li, Formation of p–n junction by plasma spraying technique to enhance the photocatalytic activity of TiO_2, Journal of Materials Science 39 (2004) 353–357.

[35] L. Cui, F. Huang, M. Niu, L. Zeng, J. Xu, Y. Wang, A visible light active photocatalyst: nano-composite with Fe-doped anatase TiO_2 nanoparticles coupling with TiO_2(B) nanobelts, Journal of Molecular Catalysis A: Chemical 326 (2010) 1–7.
[36] F. Shen, W. Que, Y. Liao, X. Yin, Photocatalytic activity of TiO_2 nanoparticles sensitized by $CuInS_2$ quantum dots, Industrial & Engineering Chemistry Research 50 (2011) 9131–9137.
[37] C.Y. Wang, D.W. Bahnemann, J.K. Dohrmann, A novel preparation of iron-doped TiO_2 nanoparticles with enhanced photocatalytic activity, Chemical Communications (2000) 1539–1540.
[38] J.X. Li, J.H. Xu, W.L. Dai, H.X. Li, K.N. Fan, Direct hydro-alcohol thermal synthesis of special core–shell structured Fe-doped titania microspheres with extended visible light response and enhanced photoactivity, Applied Catalysis, B 85 (2009) 162–170.
[39] M. Gratzel, R.F. Howe, Electron paramagnetic resonance studies of doped TiO_2 colloids, Journal of Physical Chemistry 94 (1990) 2566–2572.
[40] B. Xin, Z. Ren, P. Wang, Study on the mechanisms of photoinduced carriers separation and recombination for Fe^{3+}–TiO_2 photocatalysts, Applied Surface Science 253 (2005) 4390–4395.
[41] K.Q. Tan, H.R. Zhang, C.F. Xie, H.W. Zheng, Y.Z. Gu, Visible-light absorption and photocatalytic activity in molybdenum- and nitrogen-codoped TiO_2, Catalysis Communications 11 (2010) 331–335.
[42] J.F. Lei, X.P. Li, W.S. Li, Photocatalytic degradation of methyl orange on arrayed porous iron-doped anatase TiO_2, Journal of Solid State Electrochemistry 16 (2012) 625–632.
[43] C.C. Yen, D.Y. Wang, L.S. Chang, Characterization and photocatalytic activity of Fe- and N-co-deposited TiO_2 and first-principles study for electronic structure, Journal of Solid State Chemistry 184 (2011) 2053–2060.
[44] Z.B. Zhang, C.C. Wang, R. Zakaria, Role of the paticle size in nanocrystalline TiO_2-based photocatalysts, Journal of Physical Chemistry B 102 (1998) 10871–10878.
[45] Y. Liu, J.H. Wei, R. Xiong, C.X. Pan, The synthetic effects of iron with sulfur and fluorine on photoabsorption and photocatalytic performance in codoped TiO_2, Applied Surface Science 257 (2011) 8121–8126.
[46] S. Liu, Y.S. Chen, Enhanced photocatalytic activity of TiO_2 powders doped by Fe unevenly, Catalysis Communications 10 (2009) 894–899.
[47] S. Liu, X.P. Liu, Y.S. Chen, R.Y. Jiang, A novel preparation of highly active iron-doped titantia photocatalysts with a p–n junction semiconductors structure, Journal of Alloys and Compounds 506 (2010) 877–882.
[48] B. Erdem, R.A. Hunsicker, G.W. Simmons, XPS and FTIR surface characterization of TiO_2 particles used in polymer encapsulation, Langmuir 17 (2001) 2664–2669.
[49] Q.Q. Wang, S.H. Xu, F.L. Shen, Preparation and characterization of TiO_2 photocatalysts co-doped with iron(III) and lanthanum for the degradation of organic pollutants, Applied Surface Science 257 (2011) 7671–7677.
[50] Z. Zhang, V.E. Henrich, Electronic interactions in the vanadium/TiO_2(110) and vanadia/TiO_2(110) model catalyst systems, Surface Science 277 (1992) 263–272.
[51] J.F. Zhu, Z.G. Deng, F. Chen, Hydrothermal doping method for preparation of Cr^{3+}-TiO_2 photocatalysts with concentration gradient distribution of Cr^{3+}, Applied Catalysis B 62 (2006) 329–335.
[52] L.G. Devi, S.G. Kumar, B.N. Murthy, Influence of Mn^{2+} and Mo^{6+} dopants on the phase transformations of TiO_2 lattice and its photocatalytic activity under solar illumination, Catalysis Communications 10 (2009) 794–798.
[53] S.L. Gregg, K.S.W. Sing, Adsorption Surface Area and Porosity, Academic Press, London, 1982.
[54] M.H. Zhou, J.G. Yu, B. Cheng, H.G. Yu, Preparation and photocatalytic activity of Fe-doped mesoporous titanium dioxide nanocrystalline photocatalysts, Materials Chemistry and Physics 93 (2005) 159–163.
[55] L. Li, C. Liu, Y. Liu, Study on activities of vanadium (IV/V) doped TiO_2(R) nanorods induced by UV and visible light, Materials Chemistry and Physics 113 (2009) 551–557.
[56] N.D. Abazovic, L. Mirenghi, I.A. Jankovic, N. Bibic, D.V. Sojic, B.F. Abramovic, M.I. Comor, Synthesis and characterization of rutile TiO_2 nanopowders doped with iron ions, Nanoscale Research Letters 4 (2009) 518–525.
[57] C. Mercado, Z. Seeley, A. Bandyopadhyay, S. Bose, J.L. McHale, Photoluminescence of dense nanocrystalline titanium dioxide thin films: effect of doping and thickness and relation to gas sensing, ACS Applied Materials and Interfaces 3 (2011) 2281–2288.
[58] M.M. Rahman, K.M. Krishna, T. Soga, T. Jimbo, M. Umeno, Optical properties and X-ray photoelectron spectroscopic study of pure and Pb-doped TiO_2 thin films, Journal of Physics and Chemistry of Soilds 60 (1999) 201–210.
[59] J.K. Zhou, Y.X. Zhang, X.S. Zhao, A.K. Ray, Photodegradation of benzoic acid over metal-doped TiO_2, Industrial & Engineering Chemistry Research 45 (2006) 3503.
[60] M.I. Litter, J.A. Navfo, Photocatalytic properties of iron-doped titania semiconductors, Journal of Photochemistry and Photobiology A 98 (1996) 171–181.
[61] W.Y. Choi, A. Termin, M.R. Hoffmann, The role of metal ion dopants in quantum-sized TiO_2:correlation between photoreactivity and charge carrier recombination dynamics, Journal of Physical Chemistry 98 (1994) 13669–13679.
[62] H. Zhang, X. Lv, Y. Li, Y. Wang, J. Li, P_{25}-Graphene composite as a high performance photocatalyst, ACS Nano 4 (2009) 380–386.
[63] L.C. Liau, C.C. Lin, Fabrication and characterization of Fe^{3+}-doped titania semiconductor electrodes with p–n homojunction devices, Applied Surface Science 253 (2007) 8798–8801.
[64] J.M. Herrmann, J. Disdier, G. Deo, I.E. Wachs, Semiconductive and redox properties of V_2O_5/TiO_2 catalysts, Journal of the Chemical Society, Faraday Transactions 93 (1997) 1655–1660.
[65] S.F. Chen, X.L. Yu, H.Y. Zhang, W. Liu, Preparation and photocatalytic activity evaluation of composite Fe-TiO_2/TiO_2 photocatalyst, Journal of the Electrochemical Society 157 (2010) k96–k102.
[66] A.R. Bally, E.N. Korobeinikova, P.E. Schmid, F. Levy, Structure and electrical properties of Fe-doped TiO_2 thin films, Journal of Physics D Applied Physics 31 (1998) 1149–1154.
[67] M. Radecka, M. Rekas, K. Zakrzewska, Electrical and optical properties of undoped and Fe-doped TiO_2 single crystals, Solid State Phenomena 39-40 (1994) 113–116.
[68] O.W. Johnson, W.D. Ohlsen, P.I. Kingsbury, Defects in rutile III optical and properties of impurities and charge carriers, Physical Review Letters 175 (1968) 1102–1109.
[69] R.A. Smith, Semiconductors, 2nd ed., Cambridge University Press, London, 1978.
[70] M. Ichimura, Calculation of band offsets at the CdS/SnS heterojunction, Solar Energy Materials and Solar Cells 93 (2009) 375–378.